Journal of Solid State Chemistry 297 (2021) 122034

Contents lists available at ScienceDirect

Journal of Solid State Chemistry

journal homepage: www.elsevier.com/locate/jssc

Dehydrogenation of sodium borohydride using cobalt embedded zeolitic imidazolate frameworks

Hani Nasser Abdelhamid

Advanced Multifunctional Materials Laboratory, Department of Chemistry, Assiut University, 71516, Assiut, Egypt

ARTICLE INFO

Keywords:
Metal-organic frameworks
Zeolitic imidazolate frameworks
Hierarchical porous materials
Hydrogen

ABSTRACT

In the last decades were witnesses that hydrogen is in the limelight as an environmentally benign and alternative energy source to fossil fuels. The hydrolysis of sodium borohydride ($NaBH_4$) is promising for the synthesis of materials/chemical compounds and on-demand hydrogen generation-based applications. Herein, cobalt embedded zeolitic imidazolate frameworks (Co@ZIF-8) were synthesized at ambient temperature via a one-pot method (within 60 min). X-ray diffraction (XRD) pattern ensures the successful synthesis of a pure phase of Co@ZIF-8 crystals. Transmission electron microscope (TEM) and nitrogen (N_2) adsorption-desorption isotherm reveal that Co@ZIF-8 has a hierarchical porous structure. Co@ZIF-8 exhibited high catalytic activity for the hydrolysis of $NaBH_4$ with a hydrogen generation rate (HGR) of 7230 $mL \bullet g_{cat}^{-1} \bullet min^{-1}$ (18×10^6 $mL \bullet g_{Co}^{-1} \bullet min^{-1}$). The high catalytic performance and the simple synthesis procedure of Co@ZIF-8 endow the material's high potential to be a catalyst for hydrogen generation via the hydrolysis of hydrides such as $NaBH_4$.

1. Introduction

Zeolitic imidazolate frameworks (ZIFs) [1–3] are a subclass of metal-organic frameworks (MOFs) [4–13] with high thermal and chemical stability [14]. Among several ZIFs, ZIF-8 (zinc imidazolate) has been used as a substrate to encapsulate and support several species such as enzyme horseradish peroxidase and magnetic nanoparticles [15], achiral Cu_xS [16], cobalt [17], dye [18,19], polysaccharides [20], and aggregation-induced emission molecule [21]. It can also proceed into film/carbon cloth [22], membrane [23,24], and three-dimension (3D) product [25]. It has been applied for several applications, including catalysis, biomedicine, energy, and environmental-related fields [19, 25–33].

Hydrogen (H_2) gas is promising as an alternative energy source to fossil fuel with high energy content and environmental byproducts (e.g., H_2O) after combustion [34]. It can be used for portable electronic devices and proton exchange membrane fuel cell (PEMFC). Several companies such as Toyota, Hyundai, and Honda have recently marketed small H_2-powered vehicles [34]. It can also be used for environmental applications such as dye degradation [35] and reducing nitrophenol compounds [36–38]. There are several methods for hydrogen production [39–47]. Among these methods, hydrides' hydrolysis (1 mol $NaBH_4$ produces 4 mol H_2) offers several advantages. $NaBH_4$ has high hydrogen storage (gravimetric weight 10.6%) compared to other materials. $NaBH_4$ has lightweight/volume and produces hydrogen with high purity. The process can be controllable and produces hydrogen for on-demand uses. However, the process is kinetically slow and requires a catalyst to promote the process [48–51]. Thus, several materials were investigated as catalysts for hydrogen generation via the hydrolysis of $NaBH_4$ [52]. The high cost of precious metal catalysts, e.g., Ru, Pt, and Pd, limit their applications as catalysts for the hydrolysis of $NaBH_4$ [53]. On the other side, transition metals are cheap and offer comparable efficiency [54]. The use of transition metals requires support to enhance the performance and prevent aggregation of the active catalytic species. ZIFs are adequate supports for transition metals than other supports such as MXene, MoS_2, and carbon nanotubes (CNTs) [55–57]. However, further explorations are highly required to improve their efficiency.

Herein, the synthesis of cobalt encapsulated hierarchical porous ZIF-8 (Co@ZIF-8) has been reported. The synthesis procedure is simple using a one-pot at ambient temperature. The reaction takes place in water without the need for any organic solvent. The application of the synthesized materials for the generation of hydrogen via the hydrolysis of $NaBH_4$ was reported. Co@ZIF-8 material exhibited high catalytic activity compared to other previously reported materials.

2. Materials and methods

2-methylimidazole (Hmim), $Zn(NO_3)_2 \cdot 6H_2O$, sodium hydroxide,

E-mail address: hany.abdelhamid@aun.edu.eg.

https://doi.org/10.1016/j.jssc.2021.122034
Received 3 January 2021; Received in revised form 27 January 2021; Accepted 31 January 2021
Available online 5 February 2021

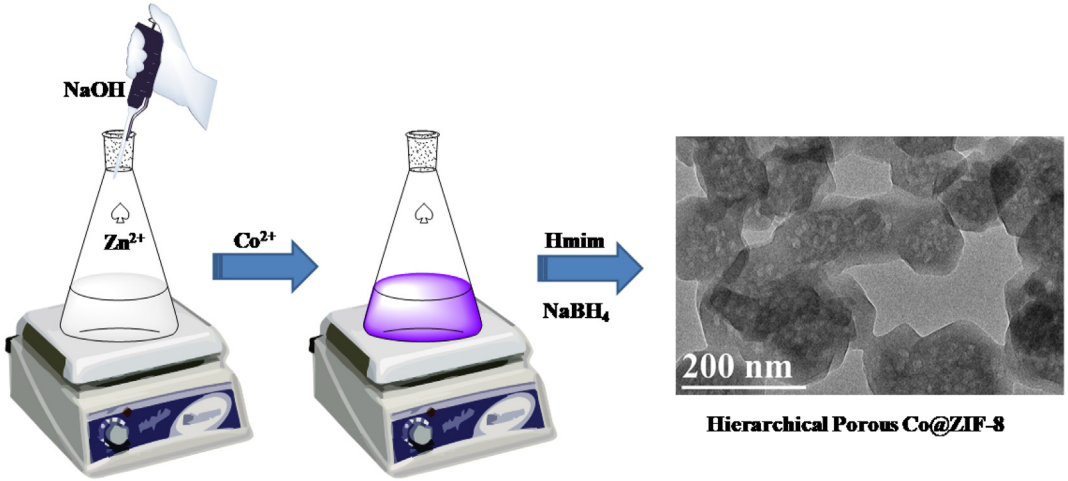

Fig. 1. Schematic representation for the synthesis of Co@ZIF-8.

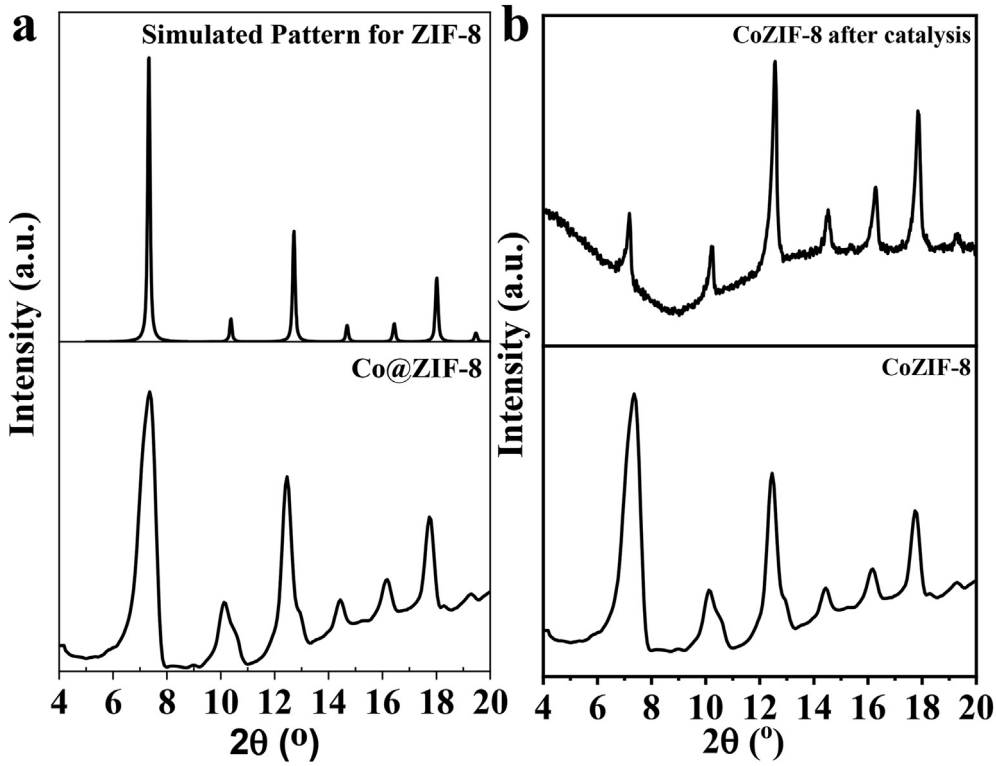

Fig. 2. a) XRD patterns Co@ZIF-8 and simulated XRD for ZIF-8, and b) Co@ZIF-8 before and after catalysis.

cobalt chloride ($CoCl_2$), were purchased from Sigma Aldrich (Germany). $NaBH_4$ was purchased from Alfa Aeser (UK).

2.1. Synthesis of Co@ZIF-8

A solution of NaOH (0.4 mL, 0.1 M) was added to a $Zn(NO_3)_2$ solution (3.2 mL, 0.84 M) at ambient conditions. A white gel was observed. Then, a $CoCl_2$ solution (0.64 g) was added. The solution was subjected to stirring for 10 min before the addition of Hmim (32 mL, 3 M). The reaction solution was continuously stirred for 30 min. A solution of $NaBH_4$ (10 mmol) was added for the reduction of Co^{2+} to Co. The product was separated using filtration and washed several times with water and ethanol to remove unreacted species.

2.2. Characterizations instruments

The crystal phase purity of Co@ZIF-8 was approved using X-ray diffraction (XRD, Philips1700 diffractometer) with wavelength, current, and accelerating voltage (V_{ac}) of 1.54 Å, 40 mA, and 40 V, respectively. Imaging was performed using transmission electron microscopy (TEM, JEM-2100, JEOL, Japan, V_{ac} 200 kV). X-ray photoelectron spectroscopy (XPS) was measured using Thermo Fischer (K-alpha, monochromated, Al K_α radiation, 1486.6 eV). The content of cobalt in Co@ZIF-8 was measured using the atomic absorption flame (AAF, Buck scientific 210 VGC). For this measurement, Co@ZIF-8 was dissolved in a strong nitric acid using ultrasonication. Surface areas (Brunauer–Emmett–Teller (S_{BET}), and Langmuir specific surface areas (S_{Lang})) and pore volumes of

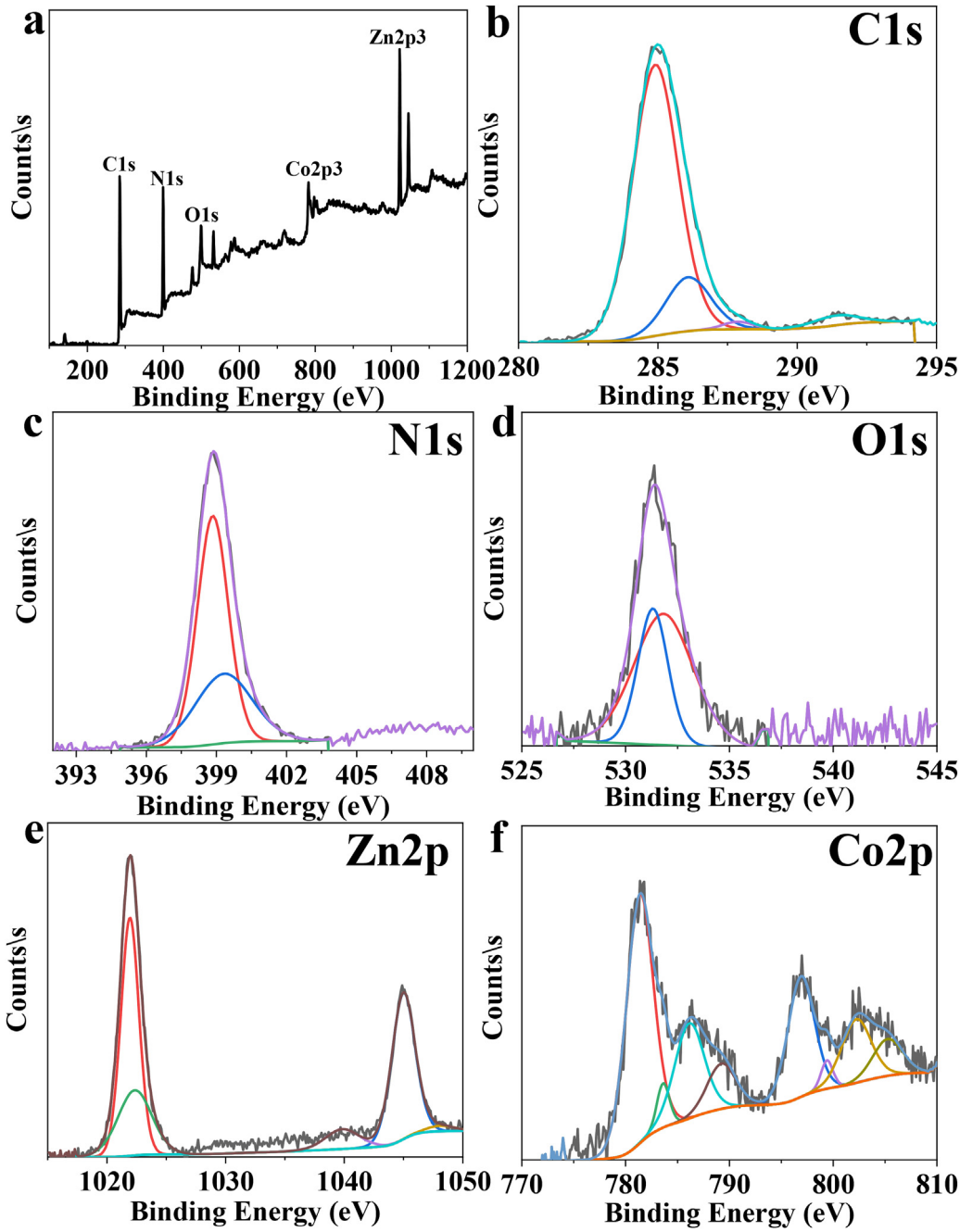

Fig. 3. XPS analysis of Co@ZIF-8, a) survey, b) C1s, c) N1s, d) O1s, e) Zn2p, and f) Co2p.

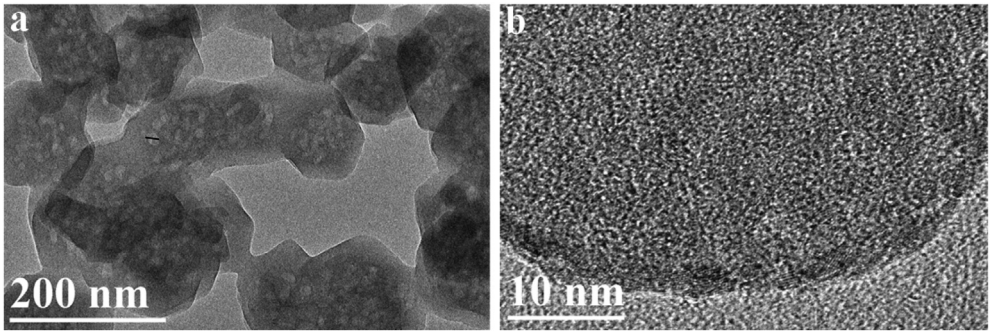

Fig. 4. a) TEM and b) HR-TEM of Co@ZIF-8.

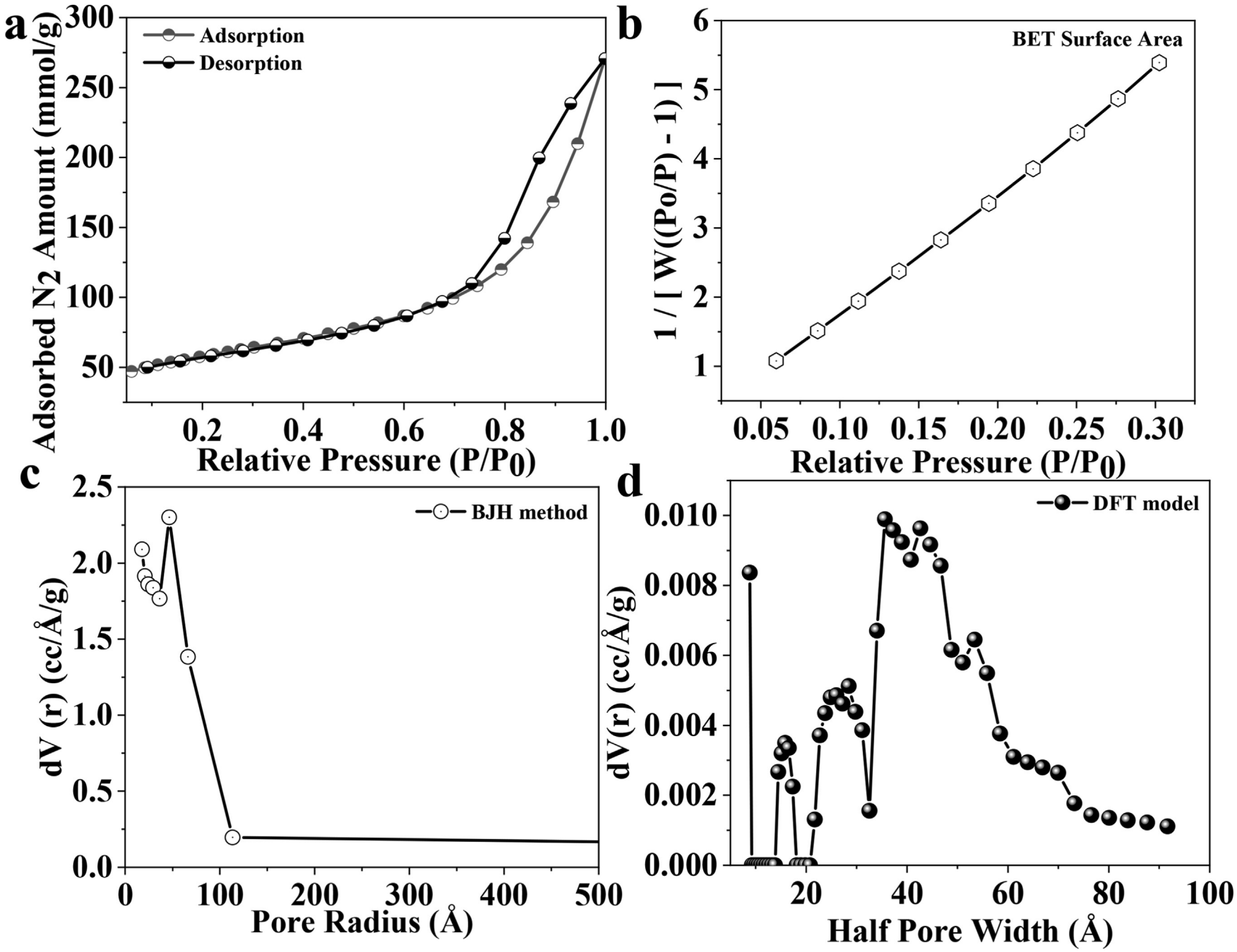

Fig. 5. a) Nitrogen adsorption-desorption isotherm, b) BET surface area fitting, pore size distribution using c) BJH model, and d) DFT model.

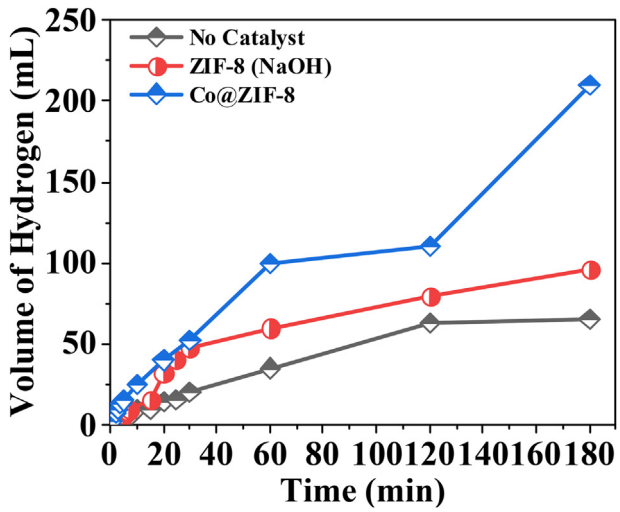

Fig. 6. The hydrolysis of $NaBH_4$ without and with Co@ZIF-8.

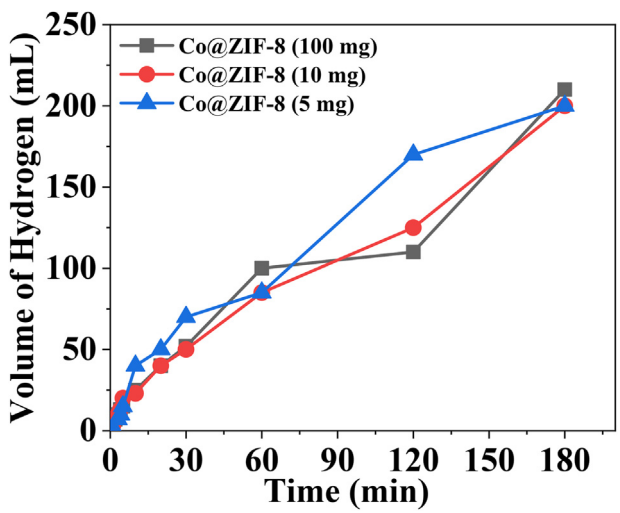

Fig. 7. The effect of Co@ZIF-8 loading on hydrogen generation via $NaBH_4$ hydrolysis.

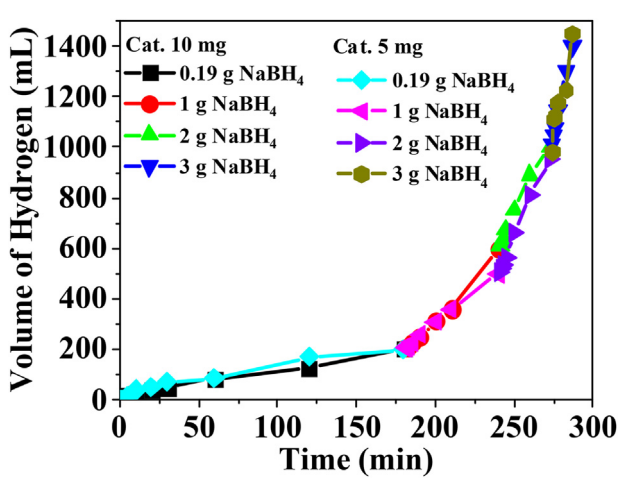

Fig. 8. The effect of $NaBH_4$ amount on hydrogen generation via $NaBH_4$ hydrolysis using Co@ZIF-8 of 5 and 10 mg.

Co@ZIF-8 were carried using a nitrogen adsorption-desorption analyzer (Quantachrome Instrument Corporation, USA, at 77 K). Co@ZIF-8 was degassed at 100 °C for 3 h under vacuum before measurements. The external surface area (S_{Ext}) was determined using the t-plot method. BJH method (Barrett, Joyner, and Halenda) and Density functional theory (DFT) models were used to evaluate the pore size distribution.

2.3. Hydrolysis of $NaBH_4$

The hydrolysis of $NaBH_4$ solution (0.19 g in 100 mL H_2O) was tested at 30 °C. The water displacement method was used to measure the hydrogen generated volume during the reaction [58]. Hydrogen was exhausted through a Tygon tube to an inverted graduated cylinder .Co@ZIF-8 (100 mg) was added to a $NaBH_4$ solution (0.19 g in 100 mL of water) following the same setup.

The effect of Co@ZIF-8 catalyst loading was investigated using catalyst loading of 100 mg, 10 mg, and 5 mg following the same experiment setups. Investigation of the impact of $NaBH_4$ amount was also tested for 0.19 g, 1 g, 2 g, and 3 g using 10 mg, and 5 mg of Co@ZIF-8. After a specific time, the reaction flask was recharged with $NaBH_4$ without catalyst separation. The hydrogen generation rate (HGR) was calculated by the active cobalt catalyst's per unit weight and was defined as $mL \bullet min^{-1} \bullet g^{-1}_{catalyst}$.

3. Results and discussion

3.1. Materials characterization

The synthesis of Co@ZIF-8 was achieved at room temperature in an aqueous solution (Fig. 1). NaOH converts zinc nitrate to a white precipitate of zinc hydroxide nitrate [59]. A violet precipitate was formed after the addition of the Hmim solution. XRD pattern of the formed violet color precipitate is reported, as shown in Fig. 2. The XRD patterns of the synthesized materials and the simulated pattern of ZIF-8 are overlapped very well, indicating the formation of a pure phase of ZIF-8 after the addition of Hmim (Fig. 2). The XRD peak broadening of the formed crystal is due to the small particle size of the formed crystals. According to Scherer's equation (Eq. (1)), Co@ZIF-8 has a crystallite size of 50–100 nm.

$$\tau = \frac{0.9\lambda}{\beta cos\theta} \quad (1)$$

Where: τ is the size of the crystallite; λ is the wavelength of X-ray radiation; β is the line broadening at half the maximum intensity in radians, and θ is the Bragg angle.

The XPS analysis of Co@ZIF-8 is shown in Fig. 3. The elemental XPS survey shows elements of C, N, O, Zn, and Co (Fig. 3a). XPS analysis of C1s show speaks corresponding to sp^2 (284.9 eV), –C–N (286.2 eV), and –C═N (287.8 eV, Fig. 3b). The analysis of N1s shows two peaks at 398.8 eV and 399.4 eV, which can be assigned to C═N– and C–N–, respectively (Fig. 3c). The oxygen species are due to the adsorbed water and carbonate (531.8 eV) into ZIF-8 (Fig. 3d). The XPS analysis of the Zn 2p region shows two peaks at 1021.9 and 1044.9 eV (Fig. 3e). The Co2p spectrum can be fitted to 8 peaks: 781.4 eV, 783.6 eV, 786.3 eV, 789.5 eV, 797.0 eV, 799.4 eV, 802.3 eV, and 805.3 eV (Fig. 3f). The two peaks at 781.4 eV and 797.0 eV (separated by 15 eV) can be assigned to Co 2p3/2 and Co 2p1/2, respectively (Fig. 3f). The other peaks are satellite peaks for Co 2p3/2 and Co 2p1/2. The observable satellite features at 786.3 eV refer to Co (II). These observations indicate that the reduction of Co (II) using $NaBH_4$ was incomplete or due to coordination of Co to mim. There was no peak corresponding to B (suppose to be at 187.7 eV), indicating no Co–B formation [70]. Cobalt loading in Co@ZIF-8 is 524 ppm, according to AAF analysis.

The morphology and particle size of Co@ZIF-8 were evaluated using TEM and high-resolution TEM (Fig. 4). TEM image (Fig. 4a) shows

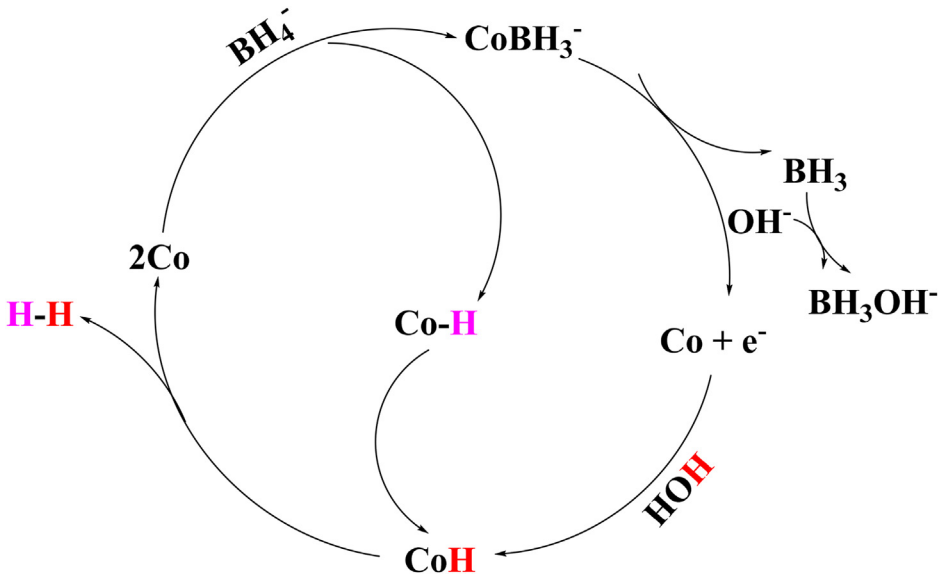

Fig. 9. Mechanism of $NaBH_4$ hydrolysis using Co@ZIF-8.

Table 1
Summary of catalysts used for hydrogen generation via $NaBH_4$ hydrolysis.

Catalyst	Synthesis Procedure	Catalysis Conditions	Rate[a]	Ref.
Co–B	$CoCl_2$ solution + $NaBH_4$ solution	0.04 M $CoCl_2$ solution, 15 wt% $NaBH_4$, 5 wt% NaOH, 30 °C	26000	[70]
Co@ZIF-8	1. Deposition-precipitation 2. In-situ reduction using $NaBH_4$	Cat. 6 mol%, $NaBH_4$, 0.75 mmol, 30 °C	2935 19400[b]	[55]
Co@ZIF-9	Solvothermal	Cat. 25 mg, $NaBH_4$, 0.5 wt%, 30 °C	3642	[63]
CoB/ZIF-8	1. Solvothermal 2. $NaBH_4$ reduction	Cat. 10 mg, $NaBH_4$ 1.67 wt%, NaOH 5 wt%	454	[56]
Co@C	1. Co-MOF-71 (24 h at 110 °C in an oven), 2. Calcination at 700 °C for 8 h under N_2 atmosphere	Cat. 20 mg, $NaBH_4$ 10 wt%, NaOH 6 wt%, 30 °C	1680	[71]
Fe_3O_4@C–Co	1. Solvothermal (200 °C, 10 h) 2. Hydrothermal (180 °C, 4 h), annealing under nitrogen, 3. Reduction with $NaBH_4$	Cat. 30 mg, $NaBH_4$ 0.26 M	1746	[62]
Co_3O_4@C	Carbonization of ZIF-67	Cat. 500 mg L^{-1}, $NaBH_4$ 4730 mg•L^{-1}; NaOH, 1 M, T = 30 °C	4900	[68]
Zn1Co1Co@NC	1. Synthesis at 120 °C for 4 h, 2. Calcination at 900 °C for 3 h	Cat. 10 mg, $NaBH_4$100 mg, NaOH 0.8 g	1807	[72]
Co@C	1. Impregnation-chemical 2. Reduction of cobalt salt using $NaBH_4$ in DMF	Cat. 20 mg, $NaBH_4$ 1 wt%; 1 wt% NaOH1 wt.%, 27 °C	10290	[67]
Co@ZIF-8	One-Pot synthesis, Room temperature,	Cat. 5 mg, $NaBH_4$ 3 wt%	7230 (18 × 10^6)[b]	Here

Notes: a, mL• min^{-1}•g^{-1}; b, mL•min^{-1}• g_{Co}^{-1}.

Co@ZIF-8 with a particle size of 50–200 nm, which agrees with the size calculated from Scherer's equation using XRD data (Fig. 2a). The formed crystals exhibited a truncated cubic crystal morphology without any observation of the aggregation of cobalt nanoparticles (Fig. 4a). The crystal contains a mesopore inside the crystal particle with a size of 5–20 nm (Fig. 4a). It is essential to mention that conventional ZIF-8 is microporous material with a pore size of fewer than 2 nm [1]. The small pore volume of microporous ZIF-8 prevents the diffusion of large molecules. On the other side, Co@ZIF-8 contains a mesopore structure as well as the micropores of conventional ZIF-8. In other words, Co@ZIF-8 is a hierarchical porous material.

Nitrogen (N_2) adsorption-desorption isotherm of Co@ZIF-8 is shown in Fig. 5a. It shows type-IV indicating the presence of micropore to mesopore regime. The analysis reveals BET surface area, Langmuir surface area, and external surface area of 200 m^2•g^{-1}, 250 m^2•g^{-1}, and 197 m^2•g^{-1}, respectively (Fig. 5b). The pore size distribution was evaluated using BJH (Fig. 5c) and DFT (Fig. 5d) model. Data analysis confirms the presence of a pore size of 3.5–25 nm with a maximum pore size 10 nm that agrees with the TEM image (Fig. 4a).

3.2. Hydrogen generation via $NaBH_4$ hydrolysis

Hydrogen generation via the hydrolysis of $NaBH_4$ using Co@ZIF-8 as a catalyst has been reported. The self-hydrolysis of $NaBH_4$ is a slow process (Fig. 6a). The production of hydrogen via $NaBH_4$ hydrolysis is kinetically limited under ambient conditions in the absence of a catalyst. Co@ZIF-8 has a large pore size and may render the diffusion of reactions feasible. Furthermore, water molecules can be dissociated into the external surface of ZIF-8 crystal, leading to acidic and basic sites [60]. Thus, Co@ZIF-8 has been investigated as a catalyst for the hydrolysis of $NaBH_4$. The generated volume of hydrogen via the self-hydrolysis of $NaBH_4$ or in the presence of ZIF-8 is low compared to the generated volume in the presence of Co@ZIF-8 materials (Fig. 6). Co@ZIF-8 can serve as an effective catalyst for the hydrolysis of $NaBH_4$ (Fig. 6).

The effect of the catalyst loading (5 mg, 10 mg, and 100 mg) was investigated, as shown in Fig. 7. There is no dramatic change in the generated volume of hydrogen for different catalyst loadings. This observation indicates that even low catalyst loading, e.g., 5 mg, can efficiently catalyze the reaction. Data reveal that Co@ZIF-8 is an effective catalyst for hydrogen generation via $NaBH_4$ hydrolysis (Fig. 7). This is mainly due to the presence of active species with high catalytic efficiency. It implies no consumption of the hydrogen generated during the

hydrolysis using a high loading of Co@ZIF-8.

The hydrolysis process depends on the reactant's concentration, i.e., water and $NaBH_4$. A large volume of water (100 mL) is used. Thus, the reaction is independent of the concentration of water, i.e., pseudo-first-order. The effect of $NaBH_4$ concentration on the generated volume of hydrogen using two different loadings of Co@ZIF-8, e.g., 5 and 10 mg, was investigated (Fig. 8). The hydrogen volume increases with the increase of $NaBH_4$ (Fig. 8). There is no dramatic difference in the efficiency of Co@ZIF-8 using 10 mg and 5 mg (Fig. 8). This observation agrees with our previous results shown in Fig. 7. The active species can be used successively without deactivation (Fig. 8).

Sodium borohydride can be recharged into the reaction solution without separating the catalyst (Fig. 8). There is no decrease in the efficiency of the catalyst over time (Fig. 8). The volume of hydrogen increases with the time and $NaBH_4$ amount (Fig. 8). The reaction becomes faster and requires a shorter time for high $NaBH_4$ loading (2–3 g). There is an insignificant difference between 10 mg and 5 mg in the catalytic performance, indicating the investigated catalyst's high performance. The hydrogen generation rates (HGR) using Co@ZIF-8 are 2961 $mL \bullet g_{cat}^{-1} \bullet min^{-1}$, and 7230 $mL \bullet g_{cat}^{-1} \bullet min^{-1}$ for 10 mg, and 5 mg, respectively (Fig. 8).

There are several studies reported that effective transition elements as catalysts for the hydride hydrolysis are used in boride or phosphide. These species are electron-rich atoms and can protect the core transition metals from oxidation via electron transfer from B to Co [61]. Thus, boride or phosphide-based catalysts alloys showed higher catalytic activity compared to the corresponding metals. However, XPS data showed no presence of B in our system, i.e., Co@ZIF-8. Several mechanisms were reported to explain the catalysis of $NaBH_4$ hydrolysis (Fig. 9). The hydrogen (4 molecules) is produced from water (2 molecules) and BH_4^- (2 molecules) (Fig. 9). The Co site and Zn metal catalyze sodium borohydride's hydrolysis and the O–H bond cleavage of H_2O (Fig. 9). The hydrolysis of $NaBH_4$ produces H_2 molecules and $BH_3(OH)^-$ (Fig. 9). Three successive processes are followed, producing $4H_2$ molecules. According to the kinetic isotope effect, the O–H bond cleavage of water is the rate-determining step [55]. It was reported that Co^{2+} ions in Co/Zn-ZIF-8 were partially *in-situ* transformed into CoB via direct reduction using $NaBH_4$ [56]. The authors reported no collapse of the ZIF-8 framework [56]. XRD pattern for Co@ZIF-8 after the hydrolysis of $NaBH_4$ indicates that the catalyst retains its basic structure after catalysis (Fig. 2b).

The synthesis procedure of Co@ZIF-8 is simple, requires no special types of equipment, occurs using water, and no need of solvothermal condition (Table 1) [56]. Among different first-raw transition metals (Fe, Co, Ni, and Cu), cobalt-based catalysts such as Co@ZIF-8 [55], Fe_3O_4@C–Co [62], and Co-ZIF-9 [63], were the most efficient and selective catalyst in this series. Cobalt offers similar reactivity to noble metals and is much more cost-effective [57,64]. Co@ZIF-8 showed a hydrogen generation rate of 14,000 $mL \bullet min^{-1} \bullet g_{Co}^{-1}$ at 30 °C [55]. However, the rapid deactivation of Co catalyst is one of the significant drawbacks of the Co-based catalyst [65]. The Co catalyst's deactivation is due to the deposition of a thick passivation layer of B–O compounds. Therefore, the catalyst should be removed and washed with a dilute acid solution for activation. A method such as encapsulation of Co NPs in carbon nanomaterials was proposed to prevent agglomeration and leaching of cobalt [66]. There is no deactivation of Co@ZIF-8 during the charging of $NaBH_4$ without the need for separation or activation process (Fig. 8). Co@ZIF-8 showed higher hydrogen generated rate compared to carbon-supported cobalt catalysts which showed hydrogen generation rate of 10290 $mL \bullet min^{-1} \bullet g_{Co}^{-1}$ at 27 °C [67]. Carbonization of ZIF-67 at 600 °C showed hydrogen generation rate (HGR) of 4900 in the presence of NaOH (1 M) [68]. On other side, Co@ZIF-8 exhibited higher hydrogen generation rate without the need for a base (Table 1). Cobalt-based catalyst suffers from rapid deactivation [69]. This could be due to nanoparticles' aggregation, degradation (for supported films/layers), or etching. Interestedly, Co@ZIF-8 can be used successfully without separation. Sodium borohydride can be recharged into the reaction mixture without the need of separation or activation steps.

4. Conclusions

A simple procedure has been reported for the synthesis of hierarchical porous Co@ZIF-8. The method was a one-pot procedure without the need for sophisticated equipment. It required a short time and uses water molecules. The reaction takes placed at ambient conditions without the need for heating. The produced material showed unique properties since it has a hierarchical porous structure. The materials exhibited high catalytic performance for hydrogen gas generation via the hydrolysis of $NaBH_4$. Co@ZIF-8 exhibited hydrogen generation rate of 7230 $mL \bullet g_{cat}^{-1} \bullet min^{-1}$ (18×10^6 $mL \bullet g_{Co}^{-1} \bullet min^{-1}$). Data may open new avenues for further exploration of effective and commercial catalysts for on-demand production of hydrogen using the hydrolysis of $NaBH_4$.

CRediT authorship contribution statement

Hani Nasser Abdelhamid: Data curation, Performed experiments, Supervision, Conceptualization, Methodology, Writing – original draft, preparation and revision, and leading the project.

Declaration of competing interest

The authors declare no competing interests.

Acknowledgment

Dr. Abdelhamid thanks Science and Technology Development Fund (STDF) for financial support (Project No 35969).

References

[1] K.S. Park, Z. Ni, A.P. Cote, J.Y. Choi, R. Huang, F.J. Uribe-Romo, H.K. Chae, M. O'Keeffe, O.M. Yaghi, Exceptional chemical and thermal stability of zeolitic imidazolate frameworks, Proc. Natl. Acad. Sci. Unit. States Am. 103 (2006) 10186–10191, https://doi.org/10.1073/pnas.0602439103.

[2] A.F. Abdel-Magied, H.N. Abdelhamid, R.M. Ashour, X. Zou, K. Forsberg, Hierarchical porous zeolitic imidazolate frameworks nanoparticles for efficient adsorption of rare-earth elements, Microporous Mesoporous Mater. 278 (2019) 175–184, https://doi.org/10.1016/j.micromeso.2018.11.022.

[3] L. Valencia, H.N. Abdelhamid, Nanocellulose leaf-like zeolitic imidazolate framework (ZIF-L) foams for selective capture of carbon dioxide, Carbohydr. Polym. 213 (2019) 338–345, https://doi.org/10.1016/j.carbpol.2019.03.011.

[4] H.N. Abdelhamid, W. Sharmoukh, Intrinsic catalase-mimicking MOFzyme for sensitive detection of hydrogen peroxide and ferric ions, Microchem. J. 163 (2021), 105873, https://doi.org/10.1016/j.microc.2020.105873.

[5] H.N. Abdelhamid, M.N. Goda, A.E.-A.A. Said, Selective dehydrogenation of isopropanol on carbonized metal–organic frameworks, Nano-Structures & Nano-Objects 24 (2020), 100605, https://doi.org/10.1016/j.nanoso.2020.100605.

[6] H.N. Abdelhamid, G.A.-E. Mahmoud, W. Sharmoukh, Correction: a cerium-based MOFzyme with multi-enzyme-like activity for the disruption and inhibition of fungal recolonization, J. Mater. Chem. B. 8 (2020), https://doi.org/10.1039/D0TB90139C, 7557–7557.

[7] H.N. Abdelhamid, G.A.-E. Mahmoud, W. Sharmouk, A cerium-based MOFzyme with multi-enzyme-like activity for the disruption and inhibition of fungal recolonization, J. Mater. Chem. B. 8 (2020) 7548–7556, https://doi.org/10.1039/D0TB00894J.

[8] M.N. Goda, H.N. Abdelhamid, A.E.-A.A. Said, Zirconium oxide sulfate-carbon (ZrOSO4@C) derived from carbonized UiO-66 for selective production of dimethyl ether, ACS Appl. Mater. Interfaces 12 (2020) 646–653, https://doi.org/10.1021/acsami.9b17520.

[9] H.N. Abdelhamid, Surfactant assisted synthesis of hierarchical porous metal-organic frameworks nanosheets, Nanotechnology 30 (2019), 435601, https://doi.org/10.1088/1361-6528/ab30f6.

[10] H.N. Abdelhamid, M. Wilk-Kozubek, A.M. El-Zohry, A. Bermejo Gómez, A. Valiente, B. Martín-Matute, A.-V. Mudring, X. Zou, Luminescence properties of a family of lanthanide metal-organic frameworks, Microporous Mesoporous Mater. 279 (2019) 400–406, https://doi.org/10.1016/j.micromeso.2019.01.024.

[11] H.E. Emam, H.N. Abdelhamid, R.M. Abdelhameed, Self-cleaned photoluminescent viscose fabric incorporated lanthanide-organic framework (Ln-MOF), Dyes Pigments 159 (2018) 491–498, https://doi.org/10.1016/j.dyepig.2018.07.026.

[12] H.N. Abdelhamid, A. Bermejo-Gómez, B. Martín-Matute, X. Zou, A water-stable lanthanide metal-organic framework for fluorimetric detection of ferric ions and tryptophan, Microchim. Acta. 184 (2017) 3363–3371, https://doi.org/10.1007/s00604-017-2306-0.

[13] H.N. Abdelhamid, Lanthanide Metal-Organic Frameworks and Hierarchical Porous Zeolitic Imidazolate Frameworks: Synthesis, Properties, and Applications, Stockholm University, Faculty of Science, 2017 https://doi.org/oai:DiVA.org:su-146398.

[14] Q. Yao, A. Bermejo Gómez, J. Su, V. Pascanu, Y. Yun, H. Zheng, H. Chen, L. Liu, H.N. Abdelhamid, B. Martín-Matute, X. Zou, Series of highly stable isoreticular lanthanide metal–organic frameworks with expanding pore size and tunable luminescent properties, Chem. Mater. 27 (2015) 5332–5339, https://doi.org/10.1021/acs.chemmater.5b01711.

[15] R. Ricco, P. Wied, B. Nidetzky, H. Amenitsch, P. Falcaro, Magnetically responsive horseradish peroxidase@ZIF-8 for biocatalysis, Chem. Commun. (2020), https://doi.org/10.1039/C9CC09358C.

[16] A. Yuan, C. Hao, X. Wu, M. Sun, A. Qu, L. Xu, H. Kuang, C. Xu, Chiral Cu_xOS@ZIF-8 nanostructures for ultrasensitive quantification of hydrogen sulfide in vivo, Adv. Mater. (2020), 1906580, https://doi.org/10.1002/adma.201906580.

[17] L. Hu, Z. Yan, X. Mo, X. Peng, L. Chen, Hierarchical Co/ZIF-8 as an efficient catalyst for cycloaddition of CO_2 and epoxide, Microporous Mesoporous Mater. 294 (2020), 109917, https://doi.org/10.1016/j.micromeso.2019.109917.

[18] H.N. Abdelhamid, Dye encapsulated hierarchical porous zeolitic imidazolate frameworks for carbon dioxide adsorption, J. Environ. Chem. Eng. 8 (2020), 104008, https://doi.org/10.1016/j.jece.2020.104008.

[19] H.N. Abdelhamid, A.M. El-Zohry, J. Cong, T. Thersleff, M. Karlsson, L. Kloo, X. Zou, Towards implementing hierarchical porous zeolitic imidazolate frameworks in dye-sensitized solar cells, R. Soc. Open Sci. 6 (2019), 190723, https://doi.org/10.1098/rsos.190723.

[20] H.N. Abdelhamid, M. Dowaidar, Ü. Langel, Carbonized chitosan encapsulated hierarchical porous zeolitic imidazolate frameworks nanoparticles for gene delivery, Microporous Mesoporous Mater. (2020), 110200, https://doi.org/10.1016/j.micromeso.2020.110200.

[21] S. Yang, S. Lu, Y. Cheng, Z. Lu, X. Liu, Y. Qin, R. Zhao, L. Zheng, Q. Cao, HDBB@ZIF-8 fluorescent nanoprobe with hereditary alcohols selectivity for chemical sensing, Microporous Mesoporous Mater. 294 (2020), 109959, https://doi.org/10.1016/j.micromeso.2019.109959.

[22] E. Asadian, S. Shahrokhian, A. Iraji Zad, ZIF-8/PEDOT @ flexible carbon cloth electrode as highly efficient electrocatalyst for oxygen reduction reaction, Int. J. Hydrogen Energy 45 (2020) 1890–1900, https://doi.org/10.1016/j.ijhydene.2019.11.124.

[23] H. Sun, Z. Magnuson, W. He, W. Zhang, H. Vardhan, X. Han, G. He, S. Ma, PEG@ZIF-8/PVDF nanocomposite membrane for efficient pervaporation desulfurization via a layer-by-layer Technology, ACS Appl. Mater. Interfaces (2020), 0c02513, https://doi.org/10.1021/acsami.0c02513 acsami.

[24] F. Chen, S. Dong, Z. Wang, J. Xu, R. Xu, J. Wang, Preparation of mixed matrix composite membrane for hydrogen purification by incorporating ZIF-8 nanoparticles modified with tannic acid, Int. J. Hydrogen Energy 45 (2020) 7444–7454, https://doi.org/10.1016/j.ijhydene.2019.04.050.

[25] S. Sultan, H.N. Abdelhamid, X. Zou, A.P. Mathew, CelloMOF: nanocellulose enabled 3D printing of metal-organic frameworks, Adv. Funct. Mater. (2018), 1805372, https://doi.org/10.1002/adfm.201805372.

[26] Y.V. Kaneti, S. Dutta, M.S.A. Hossain, M.J.A. Shiddiky, K.-L. Tung, F.-K. Shieh, C.-K. Tsung, K.C.-W. Wu, Y. Yamauchi, Strategies for improving the functionality of zeolitic imidazolate frameworks: tailoring nanoarchitectures for functional applications, Adv. Mater. 29 (2017), 1700213, https://doi.org/10.1002/adma.201700213.

[27] H.N. Abdelhamid, M. Dowaidar, M. Hällbrink, Ü. Langel, Cell penetrating peptides-hierarchical porous zeolitic imidazolate frameworks nanoparticles: an efficient gene delivery platform, SSRN Electron. J. (2019), https://doi.org/10.2139/ssrn.3435895.

[28] H.N. Abdelhamid, Z. Huang, A.M. El-Zohry, H. Zheng, X. Zou, A fast and scalable approach for synthesis of hierarchical porous zeolitic imidazolate frameworks and one-pot encapsulation of target molecules, Inorg. Chem. 56 (2017) 9139–9146, https://doi.org/10.1021/acs.inorgchem.7b01191.

[29] H.N. Abdelhamid, Biointerface between ZIF-8 and biomolecules and their applications, Biointerface Res. Appl. Chem. 11 (2021) 8283–8297, https://doi.org/10.33263/BRIAC 111.82838297.

[30] H.N. Abdelhamid, M. Dowaidar, M. Hällbrink, Ü. Langel, Gene delivery using cell penetrating peptides-zeolitic imidazolate frameworks, Microporous Mesoporous Mater. 300 (2020), 110173, https://doi.org/10.1016/j.micromeso.2020.110173.

[31] H.N. Abdelhamid, Nanoparticle-based surface assisted laser desorption ionization mass spectrometry: a review, Microchim. Acta. 186 (2019) 682, https://doi.org/10.1007/s00604-019-3770-5.

[32] H.N. Abdelhamid, Nanoparticles assisted laser desorption/ionization mass spectrometry. Handb. Smart Mater. Anal. Chem., John Wiley & Sons, Ltd, Chichester, UK, 2019, pp. 729–755, https://doi.org/10.1002/9781119422587.ch23.

[33] H.N. Abdelhamid, H.-F. Wu, Nanoparticles advance drug delivery for cancer cells, in: R.K. Keservani, A.K. Sharma (Eds.), Nanoparticulate Drug Deliv. Syst., Apple Academic Press, USA, 2019, pp. 121–150.

[34] (n.d.), https://www.wikiwand.com/en/Hydrogen vehicle, https://www.wikiwand.com/en/Hydrogen vehicle.

[35] A.A. Kassem, H.N. Abdelhamid, D.M. Fouad, S.A. Ibrahim, Hydrogenation reduction of dyes using metal-organic framework-derived CuO@C, Microporous Mesoporous Mater. 305 (2020), 110340, https://doi.org/10.1016/j.micromeso.2020.110340.

[36] A.A. Kassem, H.N. Abdelhamid, D.M. Fouad, S.A. Ibrahim, Catalytic reduction of 4-nitrophenol using copper terephthalate frameworks and CuO@C composite, J. Environ. Chem. Eng. (2020), 104401, https://doi.org/10.1016/j.jece.2020.104401.

[37] H.N. Abdelhamid, High performance and ultrafast reduction of 4-nitrophenol using metal-organic frameworks, J. Environ. Chem. Eng. (2020), 104404, https://doi.org/10.1016/j.jece.2020.104404.

[38] Y. Yang, K. Shen, J. Lin, Y. Zhou, Q. Liu, C. Hang, H.N. Abdelhamid, Z. Zhang, H. Chen, A Zn-MOF constructed from electron-rich π-conjugated ligands with an interpenetrated graphene-like net as an efficient nitroaromatic sensor, RSC Adv. 6 (2016) 45475–45481, https://doi.org/10.1039/C6RA00524A.

[39] M.N. Iqbal, A.F. Abdel-Magied, H.N. Abdelhamid, P. Olsén, A. Shatskiy, X. Zou, B. Åkermark, M.D. Kärkäs, E.V. Johnston, Mesoporous ruthenium oxide: a heterogeneous catalyst for water oxidation, ACS Sustain. Chem. Eng. 5 (2017) 9651–9656, https://doi.org/10.1021/acssuschemeng.7b02845.

[40] T. Sinigaglia, F. Lewiski, M.E. Santos Martins, J.C. Mairesse Siluk, Production, storage, fuel stations of hydrogen and its utilization in automotive applications-a review, Int. J. Hydrogen Energy 42 (2017) 24597–24611, https://doi.org/10.1016/j.ijhydene.2017.08.063.

[41] M.A. Salam, K. Ahmed, N. Akter, T. Hossain, B. Abdullah, A review of hydrogen production via biomass gasification and its prospect in Bangladesh, Int. J. Hydrogen Energy 43 (2018) 14944–14973, https://doi.org/10.1016/j.ijhydene.2018.06.043.

[42] U. Sikander, S. Sufian, M.A. Salam, A review of hydrotalcite based catalysts for hydrogen production systems, Int. J. Hydrogen Energy 42 (2017) 19851–19868, https://doi.org/10.1016/j.ijhydene.2017.06.089.

[43] K. Bolatkhan, B.D. Kossalbayev, B.K. Zayadan, T. Tomo, T.N. Veziroglu, S.I. Allakhverdiev, Hydrogen production from phototrophic microorganisms: reality and perspectives, Int. J. Hydrogen Energy 44 (2019) 5799–5811, https://doi.org/10.1016/j.ijhydene.2019.01.092.

[44] M. Anwar, S. Lou, L. Chen, H. Li, Z. Hu, Recent advancement and strategy on bio-hydrogen production from photosynthetic microalgae, Bioresour. Technol. 292 (2019), 121972, https://doi.org/10.1016/j.biortech.2019.121972.

[45] J. Jiménez-Llanos, M. Ramírez-Carmona, L. Rendón-Castrillón, C. Ocampo-López, Sustainable biohydrogen production by Chlorella sp. microalgae: a review, Int. J. Hydrogen Energy 45 (2020) 8310–8328, https://doi.org/10.1016/j.ijhydene.2020.01.059.

[46] M.S. Nasir, G. Yang, I. Ayub, S. Wang, L. Wang, X. Wang, W. Yan, S. Peng, S. Ramakarishna, Recent development in graphitic carbon nitride based photocatalysis for hydrogen generation, Appl. Catal. B Environ. 257 (2019), 117855, https://doi.org/10.1016/j.apcatb.2019.117855.

[47] M. Aslam, R. Ahmad, M. Yasin, A.L. Khan, M.K. Shahid, S. Hossain, Z. Khan, F. Jamil, S. Rafiq, M.R. Bilad, J. Kim, G. Kumar, Anaerobic membrane bioreactors for biohydrogen production: recent developments, challenges and perspectives, Bioresour. Technol. 269 (2018) 452–464, https://doi.org/10.1016/j.biortech.2018.08.050.

[48] H.N. Abdelhamid, Salts induced formation of hierarchical porous ZIF-8 and their applications for CO_2 sorption and hydrogen generation via $NaBH_4$ hydrolysis, Macromol. Chem. Phys. 221 (2020), 2000031, https://doi.org/10.1002/macp.202000031.

[49] H.N. Abdelhamid, A review on hydrogen generation from the hydrolysis of sodium borohydride, Int. J. Hydrogen Energy 46 (2021) 726–765, https://doi.org/10.1016/j.ijhydene.2020.09.186.

[50] H.N. Abdelhamid, UiO-66 as a catalyst for hydrogen production via the hydrolysis of sodium borohydride, Dalton Trans. 49 (2020) 10851–10857, https://doi.org/10.1039/D0DT01688H.

[51] H.N. Abdelhamid, Hierarchical porous ZIF-8 for hydrogen production via the hydrolysis of sodium borohydride, Dalton Trans. 49 (2020) 4416–4424, https://doi.org/10.1039/D0DT00145G.

[52] N. Patel, A. Miotello, Progress in Co–B related catalyst for hydrogen production by hydrolysis of boron-hydrides: a review and the perspectives to substitute noble metals, Int. J. Hydrogen Energy 40 (2015) 1429–1464, https://doi.org/10.1016/j.ijhydene.2014.11.052.

[53] C. Wu, J. Guo, J. Zhang, Y. Zhao, J. Tian, T.T. Isimjan, X. Yang, Palladium nanoclusters decorated partially decomposed porous ZIF-67 polyhedron with ultrahigh catalytic activity and stability on hydrogen generation, Renew. Energy 136 (2019) 1064–1070, https://doi.org/10.1016/j.renene.2018.09.070.

[54] N. Patel, B. Patton, C. Zanchetta, R. Fernandes, G. Guella, A. Kale, A. Miotello, Pd-C powder and thin film catalysts for hydrogen production by hydrolysis of sodium borohydride, Int. J. Hydrogen Energy 33 (2008) 287–292, https://doi.org/10.1016/j.ijhydene.2007.07.018.

[55] C. Luo, F. Fu, X. Yang, J. Wei, C. Wang, J. Zhu, D. Huang, D. Astruc, P. Zhao, Highly efficient and selective Co@ZIF-8 nanocatalyst for hydrogen release from sodium borohydride hydrolysis, ChemCatChem 11 (2019) 1643–1649, https://doi.org/10.1002/cctc.201900051.

[56] Q. Li, W. Yang, F. Li, A. Cui, J. Hong, Preparation of CoB/ZIF-8 supported catalyst by single step reduction and its activity in hydrogen production, Int. J. Hydrogen Energy 43 (2018) 271–282, https://doi.org/10.1016/j.ijhydene.2017.11.105.

[57] D.D. Tuan, K.-Y.A. Lin, Ruthenium supported on ZIF-67 as an enhanced catalyst for hydrogen generation from hydrolysis of sodium borohydride, Chem. Eng. J. 351 (2018) 48–55, https://doi.org/10.1016/j.cej.2018.06.082.

[58] A.A. Kassem, H.N. Abdelhamid, D.M. Fouad, S.A. Ibrahim, Metal-organic frameworks (MOFs) and MOFs-derived CuO@C for hydrogen generation from sodium borohydride, Int. J. Hydrogen Energy 44 (2019) 31230–31238, https://doi.org/10.1016/j.ijhydene.2019.10.047.

[59] H.N. Abdelhamid, X. Zou, Template-free and room temperature synthesis of hierarchical porous zeolitic imidazolate framework nanoparticles and their dye and CO_2 sorption, Green Chem. 20 (2018) 1074–1084, https://doi.org/10.1039/C7GC03805D.

[60] C. Chizallet, S. Lazare, D. Bazer-Bachi, F. Bonnier, V. Lecocq, E. Soyer, A.-A. Quoineaud, N. Bats, Catalysis of transesterification by a nonfunctionalized

Metal−Organic framework: acido-basicity at the external surface of ZIF-8 probed by FTIR and ab initio calculations, J. Am. Chem. Soc. 132 (2010) 12365–12377, https://doi.org/10.1021/ja103365s.

[61] C.-C. Yang, M.-S. Chen, Y.-W. Chen, Hydrogen generation by hydrolysis of sodium borohydride on CoB/SiO_2 catalyst, Int. J. Hydrogen Energy 36 (2011) 1418–1423, https://doi.org/10.1016/j.ijhydene.2010.11.006.

[62] A.F. Baye, M.W. Abebe, R. Appiah-Ntiamoah, H. Kim, Engineered iron-carbon-cobalt (Fe_3O_4@C-Co) core-shell composite with synergistic catalytic properties towards hydrogen generation via $NaBH_4$ hydrolysis, J. Colloid Interface Sci. 543 (2019) 273–284, https://doi.org/10.1016/j.jcis.2019.02.065.

[63] Q. Li, H. Kim, Hydrogen production from NaBH4 hydrolysis via Co-ZIF-9 catalyst, Fuel Process, Technol. 100 (2012) 43–48, https://doi.org/10.1016/j.fuproc.2012.03.007.

[64] Z. Liu, B. Guo, S.H. Chan, E.H. Tang, L. Hong, Pt and Ru dispersed on $LiCoO_2$ for hydrogen generation from sodium borohydride solutions, J. Power Sources 176 (2008) 306–311, https://doi.org/10.1016/j.jpowsour.2007.09.114.

[65] G.M. Arzac, D. Hufschmidt, M.C. Jiménez De Haro, A. Fernández, B. Sarmiento, M.A. Jiménez, M.M. Jiménez, Deactivation, reactivation and memory effect on Co–B catalyst for sodium borohydride hydrolysis operating in high conversion conditions, Int. J. Hydrogen Energy 37 (2012) 14373–14381, https://doi.org/10.1016/j.ijhydene.2012.06.117.

[66] D.-W. Zhuang, H.-B. Dai, Y.-J. Zhong, L.-X. Sun, P. Wang, A new reactivation method towards deactivation of honeycomb ceramic monolith supported cobalt–molybdenum–boron catalyst in hydrolysis of sodium borohydride, Int. J. Hydrogen Energy 40 (2015) 9373–9381, https://doi.org/10.1016/j.ijhydene.2015.05.177.

[67] W. Niu, D. Ren, Y. Han, Y. Wu, X. Gou, Optimizing preparation of carbon supported cobalt catalyst for hydrogen generation from $NaBH_4$ hydrolysis, J. Alloys Compd. 543 (2012) 159–166, https://doi.org/10.1016/j.jallcom.2012.07.099.

[68] K.-Y.A. Lin, H.-A. Chang, Efficient hydrogen production from NaBH4 hydrolysis catalyzed by a magnetic cobalt/carbon composite derived from a zeolitic imidazolate framework, Chem. Eng. J. 296 (2016) 243–251, https://doi.org/10.1016/j.cej.2016.03.115.

[69] U.B. Demirci, P. Miele, Cobalt-based catalysts for the hydrolysis of $NaBH_4$ and NH_3BH_3, Phys. Chem. Chem. Phys. 16 (2014) 6872, https://doi.org/10.1039/c4cp00250d.

[70] B. Liu, Q. Li, A highly active Co-B catalyst for hydrogen generation from sodium borohydride hydrolysis, Int. J. Hydrogen Energy 33 (2008) 7385–7391, https://doi.org/10.1016/j.ijhydene.2008.09.055.

[71] D. Xu, X. Zhang, X. Zhao, P. Dai, C. Wang, J. Gao, X. Liu, Stability and kinetic studies of MOF-derived carbon-confined ultrafine Co catalyst for sodium borohydride hydrolysis, Int. J. Energy Res. 43 (2019) 3702–3710, https://doi.org/10.1002/er.4524.

[72] Z. Gao, C. Ding, J. Wang, G. Ding, Y. Xue, Y. Zhang, K. Zhang, P. Liu, X. Gao, Cobalt nanoparticles packaged into nitrogen-doped porous carbon derived from metal-organic framework nanocrystals for hydrogen production by hydrolysis of sodium borohydride, Int. J. Hydrogen Energy 44 (2019) 8365–8375, https://doi.org/10.1016/j.ijhydene.2019.02.008.